Report: Reconstruction of Porosity Distribution

Timothé Krauth

March 15, 2025

1 Introduction

1.1 Context

Porosity is a fundamental characteristic in various scientific and engineering disciplines, significantly influencing material properties, fluid dynamics, and structural integrity. Accurate reconstruction of the three-dimensional distribution of pores is essential for applications in materials science, geophysics, and biomedical imaging [1, 2, 3]. This report presents an approach to reconstruct the three-dimensional porosity distribution of a material based on its density factor.

The dataset used in this study consists of 512 simulation instances, each corresponding to a specific density factor that defines the proportion of the volume occupied by spherical pores. The spatial domain is represented as a discretized unit cube with a resolution of $30 \times 30 \times 30$, where each grid point is assigned an occupancy flag indicating whether it lies inside a pore (1) or outside (0). Given only the density factor as input, the aim of this study is to develop an algorithm capable of accurately reconstructing the spatial distribution of pores.

To achieve this, the proposed method must efficiently infer the underlying porosity structure while maintaining computational feasibility and scalability. Figure 1 provides an illustration of a simulated grid for a density factor of 1.

1.2 Problem formulation

The task is to learn the conditional distribution $p(\mathbf{X}|d)$, where $\mathbf{X} = \{X_1, \dots, X_n\}$ represents the 3D porosity grid, n the size of the grid, and d the density factor. This distribution corresponds to the joint distribution of Bernoulli variables X_i, each indicating whether a voxel in the grid belongs to a pore. Consequently, the challenge is to estimate a high-dimensional multivariate distribution with $30 \times 30 \times 30 = 27000$ dimensions.

However, several challenges complicate the learning of this mapping:

- Curse of dimensionality: The high dimensionality of the problem may decrease the model's ability to accurately capture the dependency structure (i.e., the statistical copula) among the Bernoulli-distributed voxels based solely on the single scalar input, the density factor.
- Inherent stochasticity: As highlighted later in the literature, this problem is intrinsically stochastic. A single density factor can correspond to multiple distinct porosity grid architectures, making the learning process more complex. The model must go beyond learning a deterministic mapping and incorporate this inherent randomness.
- Sparsity of the porosity grid: The grid is highly sparse, further complicating its reconstruction. For instance, simulation `138` provides the most densely filled gird for a density factor of 1.0, with only 36% of the grid being ones. For an average density factor of 0.5, the number of ones drops to approximately 1000 out of the total $27,000$ voxels.

The combination of high dimensionality, stochastic mapping, and output sparsity makes this problem particularly challenging to solve. Therefore, the proposed method must be carefully designed to leverage the inductive biases inherent in the grid structure effectively. This report explores a novel loss function for the Variational Autoencoder to tackle with the sparsity problem, as well as incorporating structural properties of the pore distribution.

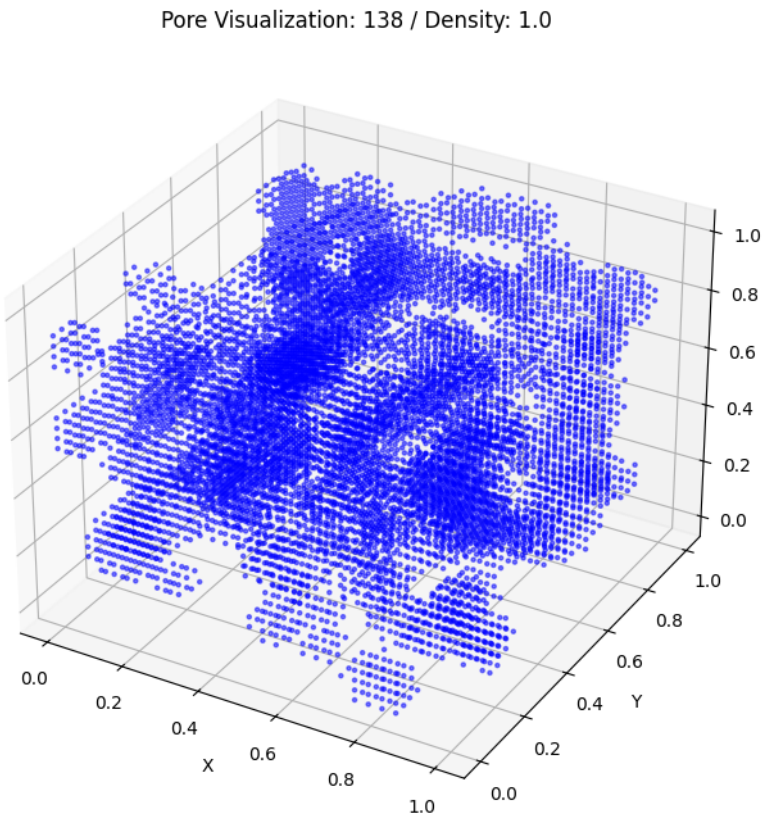

Figure 1: Example of porosity distribution for a density factor of 1.0.

In the following sections of this report, we first provide a brief literature review in Section 2, discussing conventional optimization algorithms for porosity distribution reconstruction as well as recent machine learning-based approaches. Next, Section 3 outlines the technical solutions we implemented to address the challenges. Section 4 presents the preliminary results of the study, and Section 5 its limitations. Finally, Section 6 summarizes the findings and suggests future improvements.

2 Literature Review

2.1 Conventional Algorithmic Methods

Early approaches for porosity distribution reconstruction use stochastic optimization to reconstruct a binary pore-solid structure that matches statistical descriptors such as the two-point correlation function [4]. These methods iteratively adjust a 3D grid to reproduce the porosity until convergence. They can produce realistic microstructures given sufficient descriptors, but are computationally intensive and not guaranteed to yield a unique solution as multiple distinct structures can share the same two-point correlation.

Another class of methods builds porosity distributions by packing shapes (often spheres) into a volume until a target porosity is reached. Random Sequential Addition (RSA) is a widely used algorithm for this, randomly placing non-overlapping particles sequentially [5]. RSA and related Monte Carlo packing algorithms can generate porous media with controlled volume fraction (porosity), though they may become slow at high densities as spaces for new particles diminish. Variants of RSA and sphere packing are common in materials science to simulate granular porous structures or foams, ensuring even small pores are represented.

In geoscience and reservoir modeling, Multiple-Point Statistics (MPS) algorithms reconstruct 3D porosity by sampling patterns from a training image. This geostatistical approach captures higher-order spatial relationships, reproducing complex pore connectivity beyond two-point correlations [6].

For example, a 2D thin-section image of rock can be used to stochastically generate a 3D volume with similar pore geometry. Traditional MPS ensures long-range connectivity and realistic topology (a key advantage over two-point methods) but can suffer from cumulative errors if not carefully constrained. Improved MPS techniques include porosity matching and multigrid algorithms to better preserve the training image's porosity and structural properties.

In general, the conventional algorithmic methods for porosity distribution estimation do not require extensive data for training, but rely on extensive domain knowledge (statistical descriptors or example images) and can be computationally heavy for large high-resolution volumes. As a result, they do not seem suitable for the task at hand, where only the density factor is available.

2.2 Machine Learning-based Approaches

Recent literature shows a surge in using generative models to reconstruct or synthesize 3D porous media. Generative Adversarial Networks (GANs) have been applied to learn the distribution of pore structures from tomography or microscope data and then generate new 3D realizations. [7] trained a 3D GAN on image data of bead packs and sandstones to produce high-resolution porous media samples. The GAN-generated samples were statistically representative of real media, correctly reproducing metrics like two-point correlations, pore size distributions, Euler characteristic, and even single-phase permeability. Notably, once trained, the GAN can very quickly produce multiple new pore structures that honor the training data's porosity and morphology. Other generative approaches include Deep Convolutional GANs (DCGANs) and variational autoencoders (VAEs), which have been used to reconstruct porous structures in fuel cells and batteries by learning from 3D image datasets [8]. These models can interpolate in their learned latent space to create variations of microstructures, allowing control over porosity and other features while still mimicking realistic topology.

Machine learning is also employed to predict or infer porosity distributions from indirect measurements. In geophysics, for example, deep neural networks have been trained to map seismic data or well logs to 3D porosity models, offering a data-driven alternative to physics-based inversions. [9] introduced a CNN workflow that takes multi-frequency seismic attributes as input and outputs a 3D porosity volume, achieving high prediction accuracy. Such supervised ML models learn the complex relationship between seismic response and pore structure from synthetic or historical data. They can predict fine-scale porosity details beyond the resolution of conventional methods, although they require substantial training data with known outcomes. In reservoir modeling, ensembles of regression trees and neural networks have also been used to integrate geological prior models and production data to distribute porosity in 3D, sometimes in tandem with geostatistical methods for better spatial coherence.

Emerging literature also explores combining ML with physical constraints to improve realism. For example, physics-informed GANs might ensure generated pore structures obey known laws [10], and graph neural networks have been tested to mimic grain-growth processes for scalable microstructure generation [11]. These hybrid methods aim to retain the speed of ML while respecting domain-specific constraints, thereby yielding more trustworthy reconstructions.

Given the literature, machine learning methods and more specifically deep generative models seem particularly adapted in estimated the high-dimensional porosity distribution in the given unit cube grid. Moreover, once trained, machine learning-based methods are extremely fast at producing realizations and can capture complex patterns implicitly. In the next sections we detail the methodology employed to solve this problem, given the time constraint.

3 Methodology

3.1 Data Processing

The dataset consists of 512 simulations, each represented as an array of size $(27,000, 4)$. The first three columns contain the coordinates of each voxel in the unit cube grid, while the last column is an occupancy flag indicating whether the corresponding voxel belongs to a pore. Since the unit grid is consistently sampled across all simulations, the voxel coordinates can be discarded, allowing us to reshape the arrays into binary grids of size $(30, 30, 30)$, where each entry is either 0 or 1. No additional

normalization is required, as both the grids and the density factors naturally fall within the range $[0, 1]$.

Furthermore, we observe that the density factors follow a uniform distribution, as confirmed by the 1-sample Kolmogorov-Smirnov test (we fail to reject the null hypothesis). This indicates that the dataset represents the full range of densities without any significant bias. Additionally, the number of ones in the grid can be accurately predicted from the density factor using a power-law fit, achieving an R^2 score greater than 0.996. The resulting model for the density is given by:

$$d = 0.0882 \times (\text{Number of ones})^{0.2632} \tag{1}$$

The exploration of the density factor properties is shown in Figure 2.

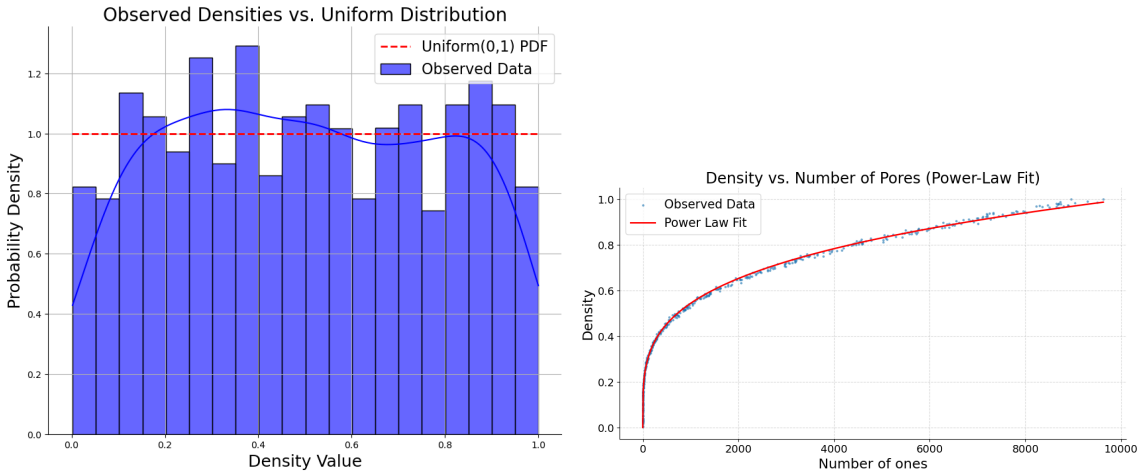

Figure 2: Density factor characteristics. Left represents the distribution of the density factor in the training dataset, whereas right represents the mapping between the density factor and the number of ones in the grid.

3.2 Model choice

Due to the curse of dimensionality and the stochastic nature of the problem, conventional machine learning methods may struggle to capture the complex dependencies between voxels. In this context, deep generative models appear particularly well-suited, as they inherently account for the stochastic variations among grids with the same density factor.

To address this challenge, we propose leveraging the Conditional Variational Autoencoder (CVAE) framework [12], a probabilistic generative model capable of learning a structured latent representation of the porosity grids. The CVAE not only captures the underlying data distribution but also enables conditional sampling with respect the density factor, making it a natural choice for modeling the relationship between density factors and porosity structures.

The VAE framework naturally aligns with the inverse problem at hand. It consists of:

- An encoder $f(\mathbf{X}) \to \mathbf{z}$, which learns the direct process, i.e., constructing lower dimensional embeddings $\mathbf{z}$ to better represent the porosity grid.
- A decoder $g(\mathbf{z}, d) \to \mathbf{X}$, which learns the inverse process, reconstructing the porosity grid from a given density factor d and a latent variable $\mathbf{z}$.

The latent space of the VAE serves as a lower-dimensional representation of the porosity grids, allowing for efficient modeling of their variability. By incorporating the density factor d into the latent space, we ensure that the generated grids align with the expected porosity level. Once the model is trained, new porosity grids can be sampled using only the decoder: a randomly drawn latent vector $\mathbf{z}$ (from the prior distribution) and a specified density factor d are fed into the decoder to generate a new grid realization.

Although only the decoder is necessary for inference, jointly training the encoder to learn the direct process can significantly improve the learning of the inverse problem, leading to more accurate and reliable grid reconstructions.

For this study, we implemented a vanilla CVAE: The prior distribution is a standard Gaussian distribution, the posterior distributions are Gaussian distributions following the mean field assumption (a diagonal covariance matrix), and the decoder distribution is assumed to follow a Bernoulli distribution.

3.3 Architecture

Given that we are working with structured 3D spatial data, 3D Convolutional Neural Networks (CNNs) are a natural choice for capturing local patterns within the grid, such as clusters of pores. Their ability to exploit spatial hierarchies makes them particularly effective for learning meaningful features from volumetric data.

Consequently, both the encoder and decoder of the VAE are implemented as 3D CNNs, with batch normalization applied between layers to stabilize training and accelerate convergence. ReLU activation functions are used throughout the network to introduce non-linearity and improve feature learning.

To ensure that the generated voxel values remain within the valid range $[0, 1]$, the decoder's output activation function is a Sigmoid. Ultimately, the decoder produces a 3D grid where each voxel represents the probability of belonging to a pore. This probabilistic output naturally accounts for the inherent stochasticity of the problem and allows for flexible thresholding during post-processing.

3.4 Loss function

3.4.1 Focal Loss

The problem can be reformulated as a multivariate binary classification task, making the Binary Cross-Entropy (BCE) loss a natural choice. However, due to the sparsity of the grids, directly applying BCE loss may lead to a bias toward predicting only zeros, as this minimizes the loss more easily. To address this issue, the loss function must be adjusted to penalize misclassifications of ones more heavily than zeros.

A straightforward approach would be to use the model described in Equation 1 to estimate the required number of ones, k, for a given density factor. One could then retain only the k largest values in the predicted grid and compare this thresholded mask with the ground truth grid. While this approach is conceptually intuitive, it suffers from a major limitation: hard thresholding is not differentiable, preventing gradients from flowing through the loss function and thus obstructing network training. Soft-relaxation alternatives are therefore required.

A possible solution involves introducing regularization techniques, such as an $L1$ penalty to enforce sparsity or a constraint ensuring that the number of ones in the reconstructed grid matches the ground truth. However, due to differences in magnitude, these penalties can be difficult to fine-tune effectively.

A more elegant and effective alternative is the Focal Loss [13]. Focal Loss builds upon BCE by dynamically down-weighting easy-to-classify examples and focusing more on hard-to-classify ones, making it particularly well-suited for handling imbalanced datasets. The Focal Loss is defined as:

$$FL(p_t) = -\alpha_t(1 - p_t)^\gamma log(p_t), \tag{2}$$

where p_t is the model's predicted probability of true class, α_t is a class weighting factor, $(1 - p_t)^\gamma$ is the focusing factor, and γ controls how much we reduce the loss for the well classified voxels.

This loss function naturally mitigates the class imbalance issue by reducing the contribution of well-classified voxels (mostly zeros) and prioritizing voxels that are harder to classify (typically the ones). As a result, it helps prevent the model from simply predicting all zeros while still learning the underlying structure of the porosity distribution.

3.4.2 Additional penalties

In addition to addressing class imbalance, we have identified two key structural properties of the grids that can be leveraged to improve learning:

- Pores never appear on the edges of the grid.

- Ones aggregate in spherical clusters rather than forming elongated or planar structures.

To incorporate these observations into the model, we introduce two additional penalty terms to the loss function, encouraging the network to respect these constraints while maintaining flexibility.

Soft Edge Penalty. While pores do not naturally appear at the boundaries of the grid, we do not wish to impose a hard constraint preventing ones near the edges. Instead, we introduce a soft edge penalty that discourages activations near the grid boundaries while still allowing them when necessary. To achieve this, we precompute a 3D distance-from-border mask that assigns higher penalty weights to voxels closer to the edges and lower weights to those near the center. During training, any predicted "1" (occupied voxel) near an edge incurs an additional loss proportional to this mask. The closer a predicted voxel is to the boundary, the larger the penalty. By adding this penalty term to the loss function, weighted by a hyperparameter λ_{edge}, the VAE is encouraged to keep activations away from edges without strictly forbidding them.

Spherical Cluster Penalty. To promote the natural tendency of pores to form spherical clusters rather than elongated or sheet-like structures, we introduce a penalty term that rewards configurations where predicted ones form dense, ball-shaped groups. We enforce this by computing a local density measure using a 3D spherical kernel convolution. The idea is that a voxel inside a well-formed spherical cluster will have many neighboring ones in all directions, whereas a voxel in a line or plane-like structure will have fewer neighbors within a given radius. We first convolve the predicted grid with a 3D spherical kernel (a binary ball of radius R) to produce a density map indicating how well a given voxel conforms to a sphere-like structure. Low-density activations are penalized, discouraging elongated structures and encouraging compact clusters. This penalty term is weighted by another hyperparameter $\lambda_{cluster}$ to balance its influence on training.

The final VAE loss function is then defined as:

$$\mathcal{L}_{VAE} = \mathcal{L}_{Focal} + \lambda_{edge}\mathcal{L}_{edge} + \lambda_{cluster}\mathcal{L}_{cluster} + \beta\mathcal{L}_{KL}, \tag{3}$$

where $\mathcal{L}_{KL}$ is the KL-divergence term from the standard VAE formulation.

3.5 Reconstruction

Due to the Sigmoid activation function, the VAE outputs a probability grid rather than a binary classification. A common approach is to apply a fixed threshold (e.g., 0.5), but this can distort the reconstructed structure, especially if probabilities are narrowly distributed.

To address this, we use the model from Equation 1 to estimate the expected number of ones based on the density factor. Instead of thresholding, we compute the expected number of ones k, sort voxel probabilities in descending order and select the top k voxels as ones, assigning zero to the rest. This adaptive approach ensures reconstructions respect the expected porosity distribution, yielding more realistic results.

4 Results

In this section, we analyze the impact of the proposed loss function on the structure of the reconstructed grid. Since we did not conduct a full hyperparameter tuning session and aim to isolate the effect of each loss component, we set the KL-loss to zero, treating the CVAE as a conventional conditional autoencoder to avoid cross-effects between the reconstruction loss and KL-divergence.

We compare reconstruction performance across three loss formulations: BCE loss, Focal Loss, and Focal Loss with additional penalty terms. Evaluation is based on visual inspection of a reconstructed grid for each loss function, the quantification of false positives (ones in prediction that should be zero), false negatives (ones in ground truth missing in prediction) and Intersection Over Union (IoU) scores as a function of the density factor.

All models were trained on 50 epochs with a latent space of dimension 256, with the ADAM optimizer and a learning rate of 10^{-5}. The encoder and decoder architectures are kept constant and consist of 3-layer 3D CNN. We divided the dataset into a training set for 90% of the samples, and a validation set of 10%. The hyperparameters for the Focal loss are $\alpha = 0.9$, $\gamma = 2$, $\lambda_{edge} = 0$,

$\lambda_{cluster} = 0$, and for the Focal loss with penalty $\alpha = 0.9$, $\gamma = 2$, $\lambda_{edge} = 0.1$, $\lambda_{cluster} = 0.3$. Figure 3 represents the IOU scores for each of the samples in the training set.

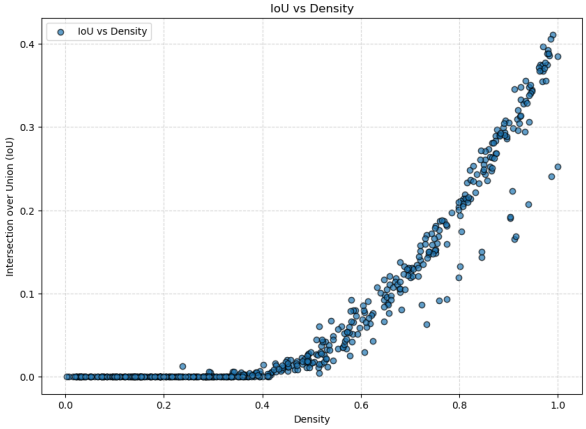

(a) IOU Score against density the using the BCE loss.

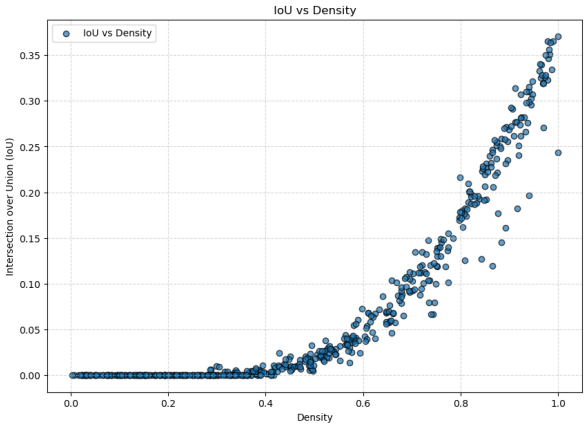

(b) IOU Score against density using the Focal loss.

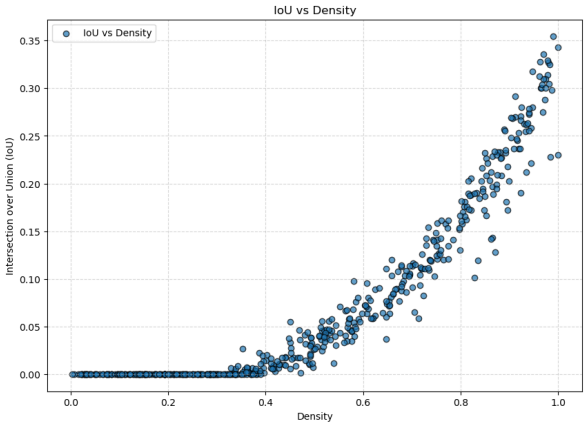

(c) IOU Score against density using the Focal loss with penalties.

Figure 3: IOU score between the ground truth grid and the reconstruction for the full dataset.

The first key observation is that IoU increases with density, not due to model performance but because of how the grids are constructed. Since we use Equation 1 to determine the number of voxels set to one, higher densities correspond to more ones, naturally leading to higher IoU scores.

However, we notice that BCE loss achieves higher IoU scores for a given density, suggesting that it is more effective at correctly placing the ones. Additionally, all methods yield IoU scores of zero at low

densities, which is expected—when only a few voxels contain ones, correctly identifying them becomes extremely difficult. This implies that, in its current state, our method fails to accurately locate pores for densities below 0.3. Interestingly, Focal Loss (with and without penalties) appears to perform slightly better in the low-density range, suggesting it might be more robust in sparse conditions.

Figure 4 shows the reconstruction for the three model for the same sample, with a density factor of 0.821. All three methods successfully identify the densest regions of ones, but they reconstruct the porosity grid with different structural patterns. The BCE loss naturally forms large clusters, which covers large portions of the expected porosity distribution. However, it also tends to create aligned regions of ones and places a significant fraction of them near the edges of the grid, making the reconstruction less realistic. This suggests that while BCE effectively learns to cluster ones, it lacks spatial constraints to prevent artifacts.

The Focal Loss without penalties improves the formation of smaller clusters, making it more consistent with the ground truth. However, this refinement comes at the cost of a lower IoU score if these clusters are not perfectly aligned with reality. Like BCE, it still produces lines of ones, indicating that without additional constraints, the model does not naturally discourage elongated structures.

The Focal Loss with penalties addresses this issue by suppressing linear structures while still forming large clusters like the BCE loss, due to the cluster penalty. It also significantly reduces the number of ones near the edges, which is a key improvement. However, this formulation introduces a new tendency: it favors the formation of dense, convex clusters in the center of the grid, making it less effective at generating smaller, scattered pores.

Strictly based on the IoU metric, the classical BCE loss appears to be the best-performing option. However, the reconstructed structures differ significantly between loss functions, indicating that IoU alone may not fully capture the quality of the reconstructions. Additionally, due to time constraints, we were unable to conduct a thorough hyperparameter tuning session, which could have significantly influenced the final results. Further optimization may reveal a better balance between accuracy and structural realism.

5 Limitations and challenges

The results indicate that BCE loss outperforms Focal Loss in terms of IoU, but this metric alone does not fully capture reconstruction quality. Several factors contribute to the limitations of the current approach, highlighting areas for improvement.

Why does BCE outperform Focal Loss? Focal Loss is designed to down-weight easy examples, allowing the model to focus on hard-to-classify voxels. However, our reconstruction method already selects the top-K highest probability voxels for binarization using Equation 1, meaning that easy and confident predictions are inherently important. If the γ parameter in Focal Loss is too high, the model may ignore too many "easy" ones, failing to reinforce correct predictions. This could explain why BCE, which treats all errors equally, ultimately achieves higher IoU scores.

Additionally, the introduction of penalties in Focal Loss makes the optimization process more unstable. The penalties impose additional constraints, causing gradients to change direction and magnitude more frequently, which can slow down learning. Since Focal Loss already weakens the gradient updates for easy examples, the combined effect with penalties leads to a weaker overall training signal compared to BCE. The model may require more training epochs or a larger learning rate to properly converge.

Hyperparameter tuning was not performed. Due to time constraints, we were unable to conduct a proper hyperparameter tuning session, which likely had a significant impact on performance. The parameters of Focal Loss (γ, α) and the weighting of penalty terms play a crucial role in the final results. A more systematic approach, such as a grid search or random search using visualization tools like Weights and Biases, could help optimize these hyperparameters for better performance.

Top-K selection may mask model performance. Our method reconstructs grids by selecting the top-K highest probability values, which ensures a realistic distribution of ones but may obscure the true performance of the reconstruction algorithm. If all predicted probabilities fall within a narrow

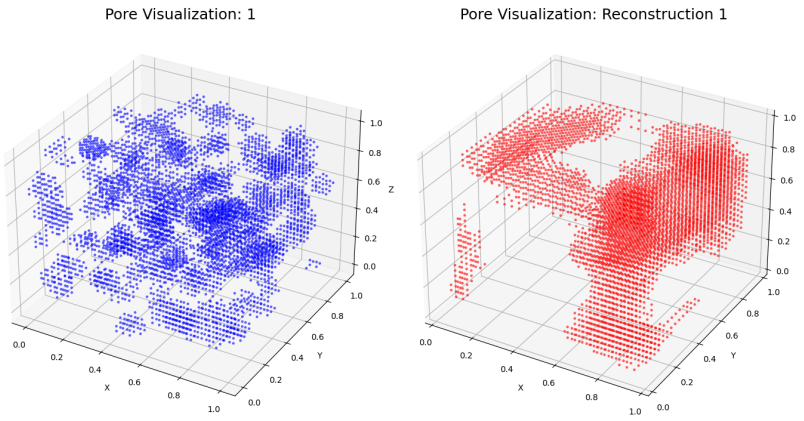

(a) Reconstruction using BCE loss. Total number of ones = 5025, false negatives = 3109, false positives = 2882, IOU score = 0.24

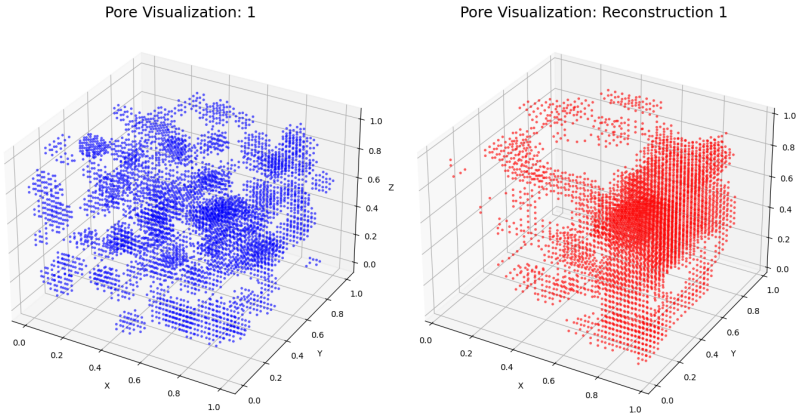

(b) Reconstruction using Focal loss. Total number of ones = 5025, false negatives = 3387, false positives = 3160, IOU score = 0.20

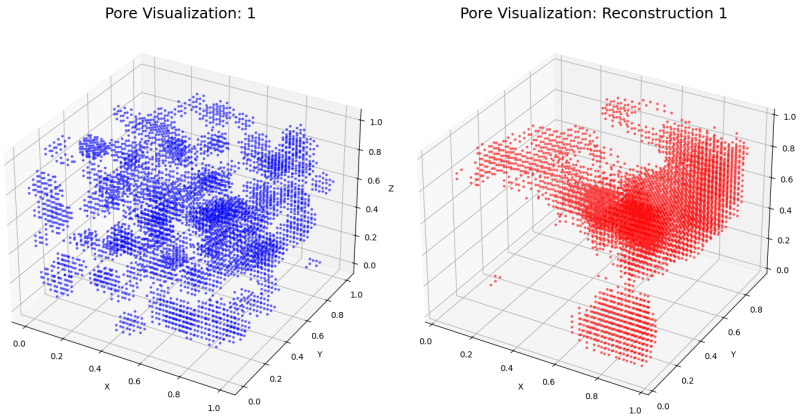

(c) Reconstruction using Focal loss with penalties. Total number of ones = 5025, false negatives = 3327, false positives = 3100, IOU score = 0.21

Figure 4: True grid for simulation number 1 (density factor of 0.821) and its Reconstruction using the three loss functions.

range (e.g., between 0.4 and 0.6), then the top-K selection may override the impact of the loss function itself. Since Focal Loss alters probability distributions by emphasizing hard examples, it may result in fewer high-confidence ones, ultimately affecting reconstruction quality. A possible improvement would be to integrate the binarization process directly into training while ensuring gradient flow remains unaffected.

IoU alone is an incomplete metric. Evaluation metrics such as IoU, false positives, and false negatives provide only a limited view of reconstruction quality, as they focus on individual voxel classification rather than overall structural realism. In some cases, grids with overly large pores may score better than those with more realistic but smaller pores, particularly at low density factors. Future work should explore more suitable evaluation metrics that assess global structure, such as Computer Vision-based metrics or density-based measures like the Wasserstein distance.

Model architecture may require improvement. The encoder-decoder architecture may not be sufficiently expressive for this problem. Interestingly, we observed that overfitting was never an issue, suggesting that the network may not be complex enough to fully capture the dataset's structure. Architectural improvements, such as adding more convolutional layers, using attention mechanisms, or increasing latent space dimensions, could improve reconstruction fidelity.

Limited dataset and missing material information The problem is inherently challenging, and the dataset provides limited information about the material properties. Currently, the model relies solely on the density factor as input, which may not provide enough information to reconstruct fine-grained structures accurately. Future improvements could involve incorporating additional material features or introducing physical inductive biases into the architecture to improve learning.

6 Conclusion

The goal of this study was to develop a machine-learning-based approach for reconstructing 3D porosity distributions given a bulk density factor. We proposed a CVAE framework with a 3D CNN encoder and decoder, trained using three different loss functions: BCE, Focal Loss, and Focal Loss with additional penalty terms. Evaluation was conducted using IoU scores, visual analysis of reconstructed grids, and the spatial distribution of predicted pore structures.

The results indicate that, in its current state, the model struggles to accurately capture the finer details of the porosity distribution, particularly at low density factors, where the reconstruction quality significantly degrades. While BCE loss achieves the best IoU scores, it fails to enforce realistic spatial structures, often placing ones along grid edges or in linear formations. Focal Loss and its penalized variant improve structure formation but introduce new trade-offs, such as slower convergence and a tendency to over-cluster ones in central regions. Additionally, the hyperparameters of the loss functions were not fine-tuned, which may have impacted performance.

A critical consideration in porosity reconstruction is uncertainty quantification (UQ), given the non-uniqueness of the inverse problem—many microstructures can share the same global porosity. Traditional stochastic methods generate ensembles of plausible realizations, while Bayesian approaches integrate prior knowledge to estimate probable pore structures. Machine learning introduces new UQ tools, particularly through generative models like GANs, VAEs, and diffusion models, which learn distributions of plausible microstructures rather than a single solution. This allows for sampling multiple realizations and assessing their variability, offering insight into the range of possible pore networks. Future work should explore integrating UQ directly into the model, ensuring that reconstructions not only match observed data but also provide confidence bounds on their accuracy.

While the current results are not fully satisfactory, this study provides a foundation for future improvements. Key directions include hyperparameter optimization, refinement of loss functions, improved network architectures, and the incorporation of additional physical constraints. By addressing these challenges, we can move toward a more accurate, reliable, and uncertainty-aware approach to porosity reconstruction.

References

[1] F. Liu, C. Song, D. Zhu, C. Li, L. Ai, C. Xin, X. Zeng, L. Zeng, N. Huang, and L. Yang, "Attrition and attrition-resistance of oxygen carrier in chemical looping process–a comprehensive review," *Fuel*, vol. 333, p. 126304, 2023.

[2] A. Mortensen and J. Llorca, "Metal matrix composites," *Annual review of materials research*, vol. 40, no. 1, pp. 243–270, 2010.

[3] M. J. De Lemos, *Turbulence in porous media: modeling and applications*. Elsevier, 2012.

[4] Y. Jiao, F. Stillinger, and S. Torquato, "Modeling heterogeneous materials via two-point correlation functions: Basic principles," *Physical Review E—Statistical, Nonlinear, and Soft Matter Physics*, vol. 76, no. 3, p. 031110, 2007.

[5] W. Xu, K. Zhang, Y. Zhang, and J. Jiang, "Packing fraction, tortuosity, and permeability of granular-porous media with densely packed spheroidal particles: monodisperse and polydisperse systems," *Water Resources Research*, vol. 58, no. 2, p. e2021WR031433, 2022.

[6] K. Ding, Q. Teng, Z. Wang, X. He, and J. Feng, "Improved multipoint statistics method for reconstructing three-dimensional porous media from a two-dimensional image via porosity matching," *Physical Review E*, vol. 97, no. 6, p. 063304, 2018.

[7] L. Mosser, O. Dubrule, and M. J. Blunt, "Reconstruction of three-dimensional porous media using generative adversarial neural networks," *Physical Review E*, vol. 96, no. 4, p. 043309, 2017.

[8] M. Delpisheh, B. Ebrahimpour, A. Fattahi, M. Siavashi, H. Mir, H. Mashhadimoslem, M. A. Abdol, M. Ghorbani, J. Shokri, D. Niblett *et al.*, "Leveraging machine learning in porous media," *Journal of Materials Chemistry A*, 2024.

[9] H. Jo, Y. Cho, M. J. Pyrcz, H. Tang, and P. Fu, "Machine learning-based porosity estimation from spectral decomposed seismic data," *arXiv preprint arXiv:2111.13581*, 2021.

[10] Z. Ren and S. Srinivasan, "Using physics informed generative adversarial networks to model 3d porous media," *arXiv preprint arXiv:2409.11541*, 2024.

[11] S. Fan, A. L. Hitt, M. Tang, B. Sadigh, and F. Zhou, "Accelerate microstructure evolution simulation using graph neural networks with adaptive spatiotemporal resolution," *Machine Learning: Science and Technology*, vol. 5, no. 2, p. 025027, 2024.

[12] C. Zhang, R. Barbano, and B. Jin, "Conditional variational autoencoder for learned image reconstruction," *Computation*, vol. 9, no. 11, p. 114, 2021.

[13] T.-Y. Lin, P. Goyal, R. Girshick, K. He, and P. Dollár, "Focal loss for dense object detection," in *Proceedings of the IEEE international conference on computer vision*, 2017, pp. 2980–2988.